Combination therapy with BMSCs-exosomes and porous tantalum for the repair of femur supracondylar defects

FAN YANG[1,2*], MINGJIAN WU[1*], HAOJIE CHEN[1], SHENGLI MA[1], JIAHE LIU[1], CHENZHI LI[1], YANCHENG LI[1], JIAHUI YANG[1], BAOYI LIU[1,2] and DEWEI ZHAO[1,2]

[1]Department of Orthopedics; [2]Postdoctoral Workstation, The Affiliated Zhongshan Hospital of Dalian University, Dalian, Liaoning 116001, P.R. China

Received October 8, 2022; Accepted April 4, 2023

DOI: 10.3892/mmr.2023.13017

Abstract. In the field of orthopedics, defects in large bones have proven challenging to resolve. The aim of the present study was to address this problem through the combination of tantalum metal (pTa) with exosomes derived from bone marrow mesenchymal stem cells (BMSCs), which have the potential to enhance regeneration of full thickness femoral bone defects in rats. Cell culture results demonstrated that exosomes improved the proliferation and differentiation of BMSCs. Following establishment of a supracondylar femoral bone defect, exosomes and pTa were implanted into the defect area. Results demonstrated that pTa acts as a core scaffold for cell adhesion and exhibits good biocompatibility. Moreover, micro-CT scan results as well as histological examination demonstrated that pTa had a significant effect on osteogenesis, with the addition of exosomes further promoting bone tissue regeneration and repair. In conclusion, this novel composite scaffold can effectively promote bone regeneration in large bone defect areas, providing a new approach for the treatment of large bone defects.

Introduction

Bone lesions due to trauma, inflammation and cancer are common in orthopedics (1,2). Currently, there are numerous methods for repairing bone defects, including bone grafting, membrane guided tissue regeneration and gene therapy. However, the efficacy of these methods for repairing bone defects is not satisfactory and the clinical outcomes when these methods are used, are not adequate to solve these problems in the clinic (3-7). Tissue engineering is a process based on principles and technologies from cell biology and material science that allows scientists to fabricate a biomaterial complex, which is used to repair a specific tissue or organ (8,9). It was reported that biological materials could be integrated with target cells or growth factors in the lab or clinic with the potential to induce bone growth (10). Thus, this process makes it possible to provide an effective approach for the treatment of large bone lesion in orthopedics.

Porous Tantalum (pTa) is a promising material for bone regeneration due to its excellent biocompatibility, osteoconductive and osseointegration properties (11,12). It has been reported that pTa has the potential to promote osteogenic differentiation of human bone marrow mesenchymal stem cells (BMSCs) and is beneficial for the attachment, growth and differentiation of human osteoblasts (13). Moreover, pTa has been reported to promote revascularization of areas of the femoral head which contain avascular necrosis, promoting cell proliferation and improving the osteogenic ability of osteoblasts (14).

BMSCs are known as seed cells in bone tissue engineering because of their excellent self-renewal and differentiation potential, as well as their ability to induce osteogenesis in *in vitro* settings (15). However, risks such as immune rejection, thrombosis, tumor formation and excessive proliferation, limits their clinical application (16-18). Exosomes are endosome-derived membrane nanovesicles with a diameter of 40-100 nm and have recently been reported to serve crucial roles in mediating intercellular communication with proteins, lipids, and genetic material such as mRNA and microRNA (miRNA) (19,20). Furthermore, exosomes are characterized by low immunogenicity, and excellent biocompatibility and biodegradability. It was previously reported that exosomes have become the preferred activator for bone repair and reconstruction (21). Critical-size bone defects are characterized as bone injuries or defects that exceed a particular size threshold, impeding the body's natural healing mechanisms and necessitating external intervention for proper bone regeneration, previous studies have demonstrated that exosomes secreted by BMSCs promote bone regeneration in a model of critical-size bone defects (22-25).

Correspondence to: Dr Baoyi Liu or Professor Dewei Zhao, Department of Orthopedics, The Affiliated Zhongshan Hospital of Dalian University, 6 Jiefang Street, Dalian, Liaoning 116001, P.R. China
E-mail: liubaoyi-513@163.com
E-mail: zhaodewei2016@163.com

*Contributed equally

Key words: porous tantalum, bone marrow mesenchymal stem cells, exosomes, bone defect, bone regeneration

The aim of the present study was to evaluate the effects of exosomes for improving osteogenic differentiation and cell proliferation. Moreover, *in vivo* pTa scaffolds combined with exosomes extracted from BMSCs were implanted into the defected regions of distal full thickness femurs in rats to assess the effect of exosomes in bone defect repair in combination with pTa.

Materials and methods

Ethics and animals. A total of 54 healthy male, specific pathogen-free (SPF) Sprague-Dawley (SD) rats (age, 6 weeks; weight 400-450 g) were used in the present study. They were purchased from the Animal Experiment Center at Dalian Medical University. The conditions under which the rats were housed during the experiment were as follows: temperature of 18-26˚C, relative humidity maintained at 40-70%, 12 h light/dark cycle, a feeding regimen with adherence to standardized formula feed, and provision of sterile and clean feed and drinking water. The animal experiments were all performed under the standards of the Animal Ethics Committee of The Affiliated Zhongshan Hospital of Dalian University (approval no. 201612009).

Isolation and culture of BMSCs. A total of 6 of the aforementioned rats were anesthetized with 1% pentobarbital sodium injected intraperitoneally (40 mg/kg) and the rats were then euthanized by dislocation of the spine. Bone marrow was subsequently harvested via gentle puncture to the tibia and femur. The total bone marrow samples were combined (~8.0 ml) and resuspended in H-DMEM (Invitrogen; Thermo Fisher Scientific, Inc.) and supplemented with 10% fetal bovine serum (FBS; Invitrogen; Thermo Fisher Scientific, Inc.), 100 UI/ml penicillin (Invitrogen; Thermo Fisher Scientific, Inc.) and 100 μg/ml streptomycin (Invitrogen; Thermo Fisher Scientific, Inc.). Cells were subsequently plated on cell culture plates for use in the studies. The cells were kept in humidified incubators at 37˚C and 5% CO_2. Cultures were rinsed with PBS (Biological Industries) after 2 days to remove nonadherent cells and fresh growth media was added. After 10-12 days, the cells reached ~80% confluence and were used in subsequent experimental studies. Growth and proliferation of BMSCs were observed using a CKX53 light microscope (Olympus Corporation).

Flow cytometry analysis of BMSCs. Flow cytometry was performed on BMSCs collected from the third passage of cell culture. Cells were washed with PBS at room temperature and subsequently suspended in 4% paraformaldehyde (Sigma-Aldrich; Merck KGaA) for 15 min. The supernatant was divided equally into five test tubes then incubated with cluster of differentiation (CD)29-FITC (1:100; cat. no. 561796; BD Pharmingen; BD Biosciences), CD34-FITC (1:200; cat. no. ab78165; Abcam), CD44-FITC (1:100; cat. no. 203906; BioLegend, Inc.), CD45-FITC (1:200; cat. no. ab33916; Abcam) or CD90-FITC (1:100; cat. no. 206105; BioLegend, Inc.) antibodies overnight at 4˚C. After cells were washed and resuspended in PBS, cell fluorescence was analyzed using a FACS Calibur flow cytometer (Becton, Dickinson and Company), and the data acquisition and analysis was performed with CytExpert (v2.4; Beckman Coulter, Inc.).

Assessment of the induction of differentiation ability of BMSCs. BMSCs ($1x10^8$/ml) from the fourth cell passage were collected and seeded in two 6-well plates. Adipogenic differentiation was induced using H-DMEN containing adipogenic inducer [20% FBS (Invitrogen; Thermo Fisher Scientific, Inc.), 5 μg/ml insulin (Sigma-Aldrich; Merck KGaA), 50 μM indomethacin (Sigma-Aldrich; Merck KGaA), 1 μM dexamethasone, 0.5 μM glutamine, 100 U/ml penicillin (Beyotime Institute of Biotechnology) and 100 μg/ml streptomycin (Beyotime Institute of Biotechnology)]. Cells were cultured at 37˚C and 5% CO_2, culture medium was changed every 2 or 3 days, and adipogenic induction was performed for 21 days in total. Then the cells were fixed in 10% formalin at room temperature for 20 min before oil red O staining to assess lipid deposition using modified oil red O staining kit (no. C0158S, Beyotime Institute of Biotechnology) for 15 min at room temperature. Osteogenic differentiation was induced using H-DMEN supplemented with osteogenic inducer [20% FBS (Invitrogen; Thermo Fisher Scientific, Inc.), 20 mM β-phosphate glycerol (Sigma-Aldrich; Merck KGaA), 1 nM dexamethasone, 50 ng/ml Thyroxine (Sigma-Aldrich; Merck KGaA), 0.5 μM Ascorbate 2-phosphate (Sigma-Aldrich; Merck KGaA), 12 mM glutamine, 100 U/ml penicillin and 100 μg/ml streptomycin]. Cells were cultured at 37˚C and 5% CO_2, culture medium was changed every 2 or 3 days, and osteogenic induction was performed for 21 days in total. To qualitatively evaluate intracellular alkaline phosphatase (ALP) activity, cells were fixed with 10% formalin for 20 min at room temperature, and stained with BCIP/NBT ALP color development kit (no. C3206, Beyotime Institute of Biotechnology) and incubated in the dark for 20 min at room temperature. The BCIP/NBT staining working solution was prepared by adding 3 ml ALP chromogenic buffer, 10 μl BCIP solution, 20 μl NBT solution according to the manufacturer's instructions.

Isolation and purification of exosomes. The present study utilized size exclusion chromatography (SEC) to isolate and concentrate exosomes, which is considered one of the optimal methods for separating and purifying exosomes from samples (26). The following procedures were performed according to the manufacturer's instructions for the SuperEV 1.0 kit (Runji Biotechnology Co., Ltd.). Briefly, BMSCs were cultured and the supernatant (1 ml) was centrifuged at 3,000 x g at 4˚C for 10 min to remove cells or cell debris. The resulting supernatant was transferred to the top of a sieve plate and a 15 ml centrifuge tube was used to collect the filtrate. After the sample was completely transferred to the sieve plate, 7 ml of PBS was added. The first fraction (~8 ml), which did not contain extracellular vesicles, was collected. The washing step was repeated with 1 ml of PBS each time until no liquid flowed out of the outlet, and each fraction was collected in 1 ml volumes. The extracellular vesicles were mainly concentrated in fractions 2-4, with a total volume of ~3 ml. The purification process of extracellular vesicles was performed as follows: the aforementioned fractions (~3 ml) were mixed with 0.3 ml binding buffer in a centrifuge tube. After thorough mixing by inversion, 200 μl of binding resin was added, and the mixture was inverted and mixed for 15 min at room temperature, followed by centrifugation at 1,500 x g at room temperature for 3 min. Then, 0.5 ml of the supernatant was

aspirated with a pipette, the resin was gently blown up, and the entire supernatant was transferred to a purification column in an equipped collection tube. The column was allowed to stand for 2 min and then centrifuged at 3,000 x g at room temperature for 2 min. The filtrate and collection tube were discarded, and the purification column was placed in a 1.5 ml centrifuge tube. A total of 200 μl of elution buffer was added to the column, and it was allowed to stand for 5 min. The column was then centrifuged at 500 x g at room temperature for 2 min, and the filtrate was added back to the column. The column was allowed to stand for 2 min, and then centrifuged at 500 x g at room temperature for 2 min. Finally, the column was centrifuged at 3,000 x g at room temperature for 2 min, and the resulting filtrate contained the concentrated exosomes. The extracted exosomes were directly used in subsequent experiments or stored at 2-8˚C for one week.

Characterization of exosomes. Using a micropipette, 20 μl of the prepared exosome suspension was deposited onto a copper grid, allowing for spontaneous adsorption over a duration of 10 min. Subsequently, surplus liquid droplets were removed using filter paper. Next, 20 μl of 2% phosphotungstic acid solution (Structure Probe, Inc.) was deposited onto the copper grid, and allowed to rest for 5 min. After which excess liquid droplets were removed using filter paper and grids were left to air dry thoroughly. Transmission electron microscopy (TEM; H7650; Hitachi, Ltd) was then performed at 80 kV to capture images.

Diluted samples (1,000 fold) in PBS were analyzed to assess the size of the exosomes using zeta view nanoparticle tracking analyzer (version, PMX110; Particle Metrix GmbH), which was calibrated using polystyrene microspheres.

Extracted exosomes were lysed in RIRF-PMSF buffer (Beyotime Institute of Biotechnology) and quantified using a BCA protein kit. Western blot was performed on these lysed extracts. After the 10% SDS-PAGE separation gel was prepared, a total of 20 μl of sample (1 mg/μl) was loaded into each well of the gel, and the gel was electrophoresed at 60 v for 30 min for the upper layer and 110 v for 120 min for the lower layer. Bands were transferred to a PVDF membrane. Next the membrane was cut and blocked with 5% skimmed milk (0.75 g milk powder + 15 ml PBS) at 37˚C for 1 h. The blocked membrane was washed with PBS-T (1,000 ml 1xPBS + 1 ml Tween-20), and then incubated with primary antibodies against TSG101 (1:1,000; cat. no. 28283-1-AP; Proteintech Group, Inc.), CD9 (1:1,000; cat. no. 20597-1-AP; Proteintech Group, Inc.), HSP70 (1:3,000; cat. no. 10995-1-AP; Proteintech Group, Inc.), and GAPDH (1:10,000; cat. no. 60004-1-Ig; Proteintech Group, Inc) overnight at 4˚C. The membrane was washed with PBST and then incubated with Goat anti-rabbit IgG (H+L)-HRP secondary antibodies (1:5,000; cat. no. 111-035-003; Jackson ImmunoResearch Laboratories, Inc.) at 37˚C for 1 h. The control group received the same treatment. The protein band images were obtained by exposing the membrane to ECL ultra-sensitive luminescence reagent (Beyotime Institute of Biotechnology) and imaged using a gel imaging system.

Differentiation and proliferation of BMSCs in vitro. BMSCs ($1x10^8$/l) at cell passages 4 and 5 were collected and inoculated on 6-well cell culture plates. Each group of cells was treated as indicated in Table I. The concentration gradient set for exosomes in the partial group and total exosome group was 50 and 100%, respectively, based on previous reports (22,23), in order to evaluate whether exosome activity was related to the concentration. A total of 2.5 ml of osteogenesis inducer (prepared according to the aforementioned method) was added to each group once every 3 days over a 21 day period. Culture fluid was discarded from each sample and samples were fixed in 10% paraformaldehyde for 20 min at room temperature and stained for 20 min at room temperature using an alizarin red S staining kit for osteogenesis (no. C0148S, Beyotime Institute of Biotechnology) and BCIP/NBT ALP color development kit. Samples were washed with PBS and examined under a light microscope for cell staining. Induced osteoblasts were cultured in L-DMEM complete medium at 37˚C and 5% CO_2 (Gibco; Thermo Fisher Scientific, Inc.) and the cell culture media was changed once every 3 days. Osteoblasts in passage 4 were seeded into 96-well plates (200 μl/well) at a concentration of $1x10^4$/ml. Each sample was divided into 3 groups as follows: i) PBS (100 μl); ii) PBS (75 μl) + BMSCs-exosome suspension (25 μl); and iii) PBS (50 μl) + BMSCs-exosome suspension (50 μl), and incubated overnight with 5% CO_2 at 37˚C. Microscopy was used to assess cell adherence after which 20 μl of CCK-8 reagent (Corning, Inc.) was added to cells. After 4 h, the absorbance value of each well was measured at a wavelength of 450 nm using a Multiskan SkyHigh microplate analyzer (Thermo Fisher Scientific, Inc.). This experiment was repeated in triplicate and the average value including standard error were recorded as the final result. Furthermore, the column diagram of the cell proliferation rates was drawn as an abscissa using proliferation rates as vertical coordinates.

Table I. Experimental grouping for assessment of the promotion of osteogenesis by exosomes *in vitro*.

Group	PBS (μl)	Exosomes suspension (μl)
Control	40	0
Partial exosomes	20	20
Total exosomes	0	40

Generation of a three-dimensional pTa scaffold. pTa materials were provided by the Orthopedics Laboratory at The Affiliated Zhongshan Hospital of Dalian University (China). pTa metal was machine-cut into flat cylinders with a diameter of 3 mm and a height of 2 mm, based on the intended shape and size of the bone defect area in the animal model. Ultrasonic cleaning of the modules was performed twice in anhydrous acetone, 70% ethanol and distilled water for 20 min each. Subsequently, they were sterilized using high pressure steam and dried before further use. Scanning electron microscopy (SEM) was used to view the pTa modules after being treated with ion sputtering using a gold spray apparatus.

Surgical procedure for in vivo studies. A total of 48 of the aforementioned healthy male SPF SD rats were randomly divided into 4 groups (n=12), the age of which were the same as those in the aforementioned *in vitro* studies section. The

Table II. Experimental grouping of the *in vivo* experiment.

Group	Abbreviation	Treatments	Quantity of exosomes (μl)
Control	NC	Full-thickness bone defect	0
pTa	PT	Full-thickness bone defect with pTa implantation	0
Exosomes	Exo	Full-thickness bone defect with exosomes	20
pTa integrated with exosomes	PE	Full-thickness bone defect with pTa integrated with exosomes	20

pTa, tantalum metal.

treatment of each group was presented in Table II. Anesthesia was delivered via intraperitoneal injection with 1% pentobarbital sodium at 40 mg/kg. The dorsal surgical sites of each rat were disinfected with iodophor solution after administration of anesthesia. A longitudinal incision ~1.5 cm in length was made in the anterior midline of the right knee joint. The joint was flexed and the patella was laterally distended to expose the inclined surface of the femoral condyle metaphyseal. A drill with diameter of 2 mm was used to drill vertically 3 mm above femoral condyle to reach the medullary bone and moved horizontally 3 mm leaving a cavity 2 mm wide, 3 mm in length and 2 mm in height, as indicated in Fig. 1A. Then, appropriate modifications were made at the site according to the experiment scheme and treatment group (Table II). Negative control (NC) group rats contained surgically drilled cavities without implantation of material. After bones cavities of the exosome group of rats were rinsed and cleaned, 0.02 ml of BMSCs-exosome suspension was dropped into the cavities of the exosomes (Exo) group. A pTa metal module was implanted in the bone cavities of rats in the pTa (PT) group. A total of 0.02 ml of BMSCs-exosome suspension was dropped onto the tantalum block using a sterile injection syringe (Fig. 1B). After the exosome suspension completely penetrated the pTa pores by standing for 20 min after dropping, they were implanted into the bone cavities of the pTa integrated with exosomes (PE) group. The incisions were sutured and the start date of the experiment was noted. In order to protect the experimental animals from unnecessary pain, humane endpoints were included in the study design, briefly: The experiment must be stopped immediately if the animals experienced unbearable pain or suffering, were subjected to inappropriate housing conditions, if the scientific purpose of the experiment was not fulfilled, if the animals were not adequately protected and cared for, or if the experiment posed serious ethical issues such as lack of sufficient approval from an animal ethics committee.

Imaging evaluation. Rats were sacrificed via cervical dislocation at 4, 8 and 12 weeks post-operation after intraperitoneal injection of 1% pentobarbital sodium at a dose of 40 mg/kg, 4 rats in each group were sacraficed at each time point. Right femur samples were collected and fixed using 10% paraformaldehyde for 48 h at room temperature. micro-CT scans (Siemens AG) were performed and visual analysis. The scanning scheme was 80 kV and 500 A with a pixel size set at 28.21 μm. Images and CT scan gray values were analyzed to evaluate bone healing for each group. Visual data were collected and

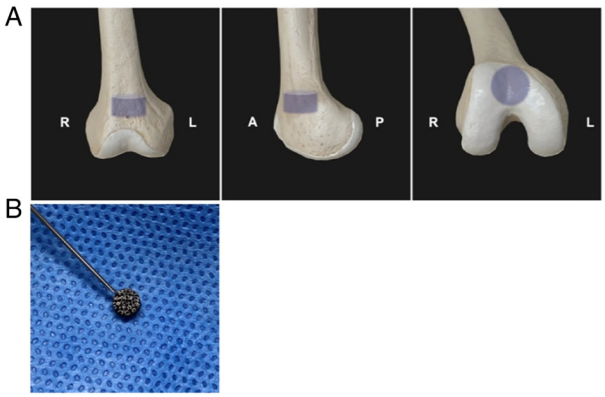

Figure 1. Schematic diagram of modeling zone and pTa loading exosomes. (A) Schematic image of the full-thickness bone defect model preparation. (B) Exosomes were loaded in a porous tantalum metal module.

reconstructed using Inveon Acquisition Workplace (v4.7, Siemens AG) and Inveon Research Workplace software (v4.1, Siemens AG).

Histomorphology. Specimens scanned via micro-CT were removed from the 10% paraformaldehyde solution and dehydrated using an increasing concentration alcohol series. Specimens were embedded in methyl methacrylate resin for tissue slicing. Sections (10 μm) were prepared from different sites in the bone for analysis using Gieson staining, which was performed as follows: Tissue sections were immersed in formic acid for 3 min and subsequently methanol for 2 h at room temperature. Tissues were washed with deionized water and incubated with methylene blue (Sigma-Aldrich; Merck KGaA) at 60˚C for 5 min. Tissue slices were washed with deionized water 3 times and subsequently stained with picric acid-magenta solution (Sigma-Aldrich; Merck KGaA) for 15 min at room temperature. Slides were washed with anhydrous ethanol and observed under x4 and x10 magnifications using a CKX53 inverted microscope.

Statistical analysis. All data were statistically analyzed using SPSS 22.0 software (IBM Corp), with quantitative data presented as mean ± standard deviation. Multiple comparisons were performed using one-way ANOVA followed by LSD/SNK analyses to determine the statistical significance between each group. $P<0.05$ was considered to indicate a statistically significant difference.

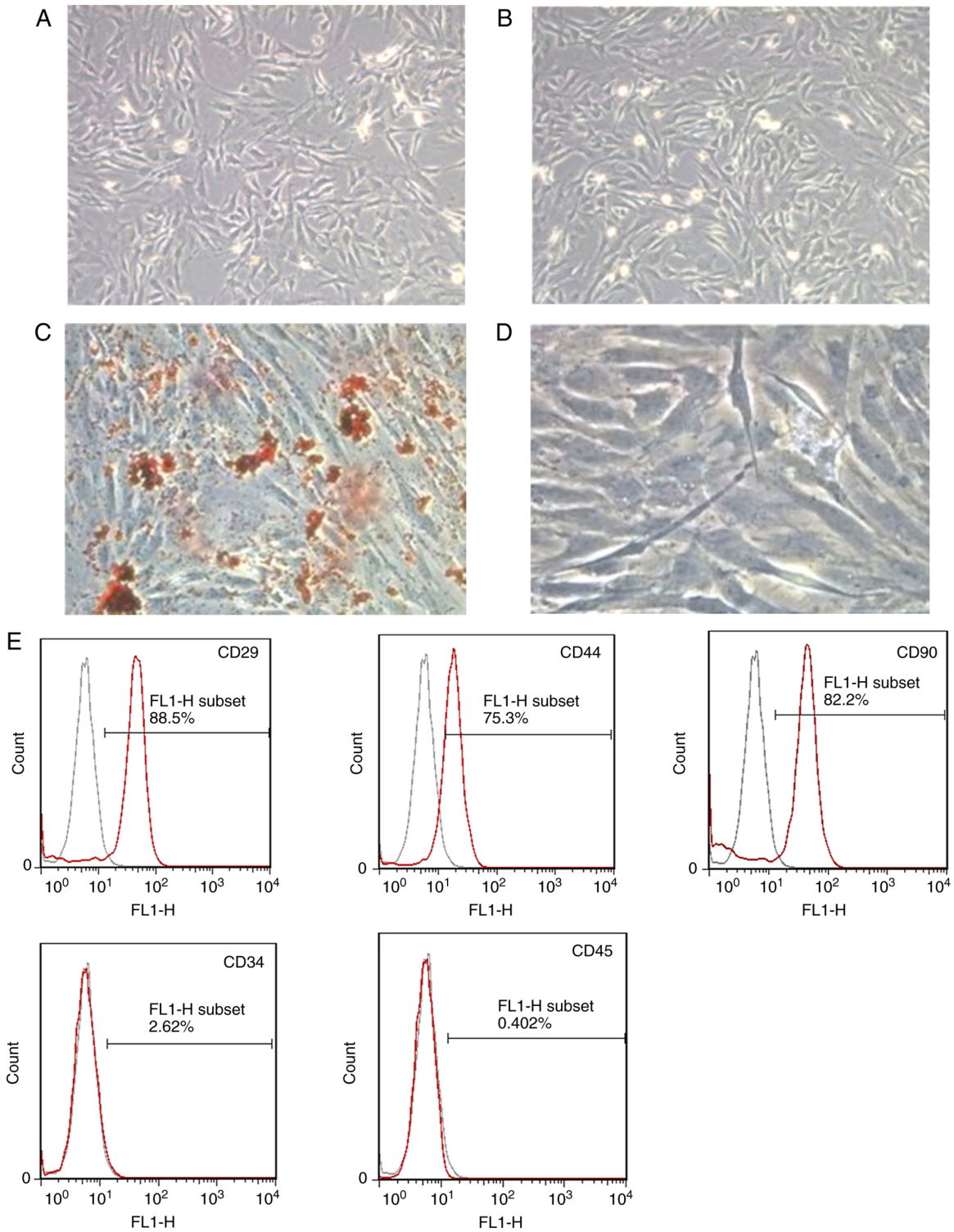

Figure 2. Identification of BMSCs. Morphological images (x100 magnification) of BMSCs cultured continuously for (A) 7 and (B) 14 days. BMSCs at 4 passages were positive for (C) oil red O staining (x200 magnification) and (D) ALP staining (x400 magnification) after 3 weeks of osteogenesis induction. (E) BMSCs surface markers expressed CD29, CD44 and CD90, and were negative for hematopoietic cell surface antigen markers CD34 and CD45.

Results

Characteristics of BMSCs. BMSCs seeded in fresh, complete culture medium were observed using an inverted microscope. Representative histological images of day 7 and day 14 were presented in Fig. 2A and B, respectively. After 7 days of cell culture, cells could be seen adhering to the walls of the culture dish and growing with varying rod-like or spindle-shaped appearances. After 14 days of cell culture, cells could be seen growing well with a uniform distribution and a single spindle or spindle-like shape. Flow cytometry was used to assess antigen surface markers and BMSCs. The cells isolated from bone marrow were demonstrated to express CD29, CD44 and CD90 at high levels, whereas minimal expression was demonstrated

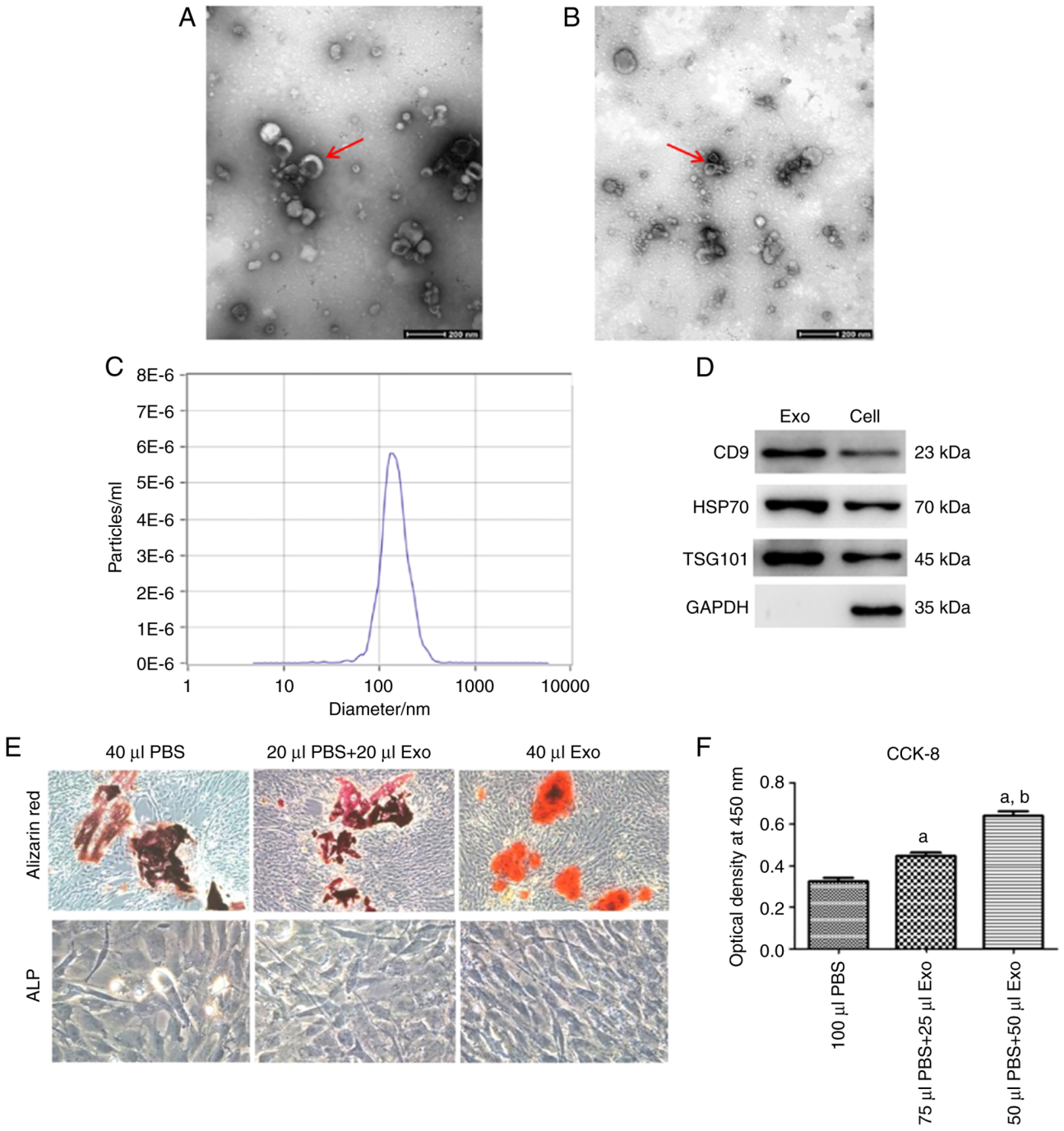

Figure 3. Identification of exosomes and their biological activity identification. (A and B) The general morphology of isolated exosomes was assessed using transmission electron microscopy. (C) The size distribution of exosome particles was assessed using nanoparticle tracking analysis. (D) Western blotting was used to assess the presence of the positive exosomal markers CD9, HSP70 and TSG101. (E) Alizarin red (x100 magnification) and ALP (x400 magnification) staining of BMSCs after treatment with exosomes and culture for 21 days. (F) Quantification of cell proliferation using the OD value of CCK-8. [a]P<0.05 compared vs. 100 μl PBS; [b]P<0.05 vs. 75 μl PBS + 25 μl Exo. ALP, alkaline phosphatase; Exo, BMSCs exosome suspension.

for CD34 and CD45 markers (Fig. 2E). These results suggested that cells extracted from bone marrow consisted of primarily BMSCs (27,28). The multipotent differentiation capacity of the extracted BMSCs was assessed by monitoring the lipid droplets and ALP deposition after adipogenic and osteogenic induction, without conducting baseline assessments. After 21 days of adipogenesis induction, red-stained lipid droplets were observed deposited inside the cells following Oil Red O staining (Fig. 2C). Furthermore, it was observed that cells extracted from bone marrow expressed ALP after osteogenic induction for 21 days (Fig. 2D). The staining results indicated that the cells isolated during the bone marrow studies potentially had the capacity for differentiation.

Identification of BSMC-exosomes. Exosomes were characterized using TEM to determine size and structure, which indicated that their structure was a cup-shaped phospholipid bilayer 40-100 nm in diameter (Fig. 3A and B). Size distribution of the exosomes was determined using nanoparticle tracking analysis (NTA). The concentration of the exosomes

was assessed to be $6.0x10^{10}$/ml, with a mode size of 142.2 nm (Fig. 3C). Western blotting results indicated that proteins extracted from these exosomes expressed traditional exosome markers, such as CD9, HSP70 and TSG101 (Fig. 3D). Taken collectively, these data suggested successful isolation of BMSCs-exosomes from the bone marrow cells.

Promotion of BMSCs-exosomes in differentiation and proliferation. Primary BMSCs were cultured with osteogenic inducer for 21 days, after which Alizarin red and ALP staining of samples was used to determine if exosome treatment could promote BMSCs differentiation (Fig. 3E). Cells cultured with 40 μl of BMSCs-exosomes demonstrated robust staining, which suggested calcium nodule formation enhancement. Samples cultured with exosomes demonstrated an overall higher degree of staining compared with the control group. Cells cultured with exosomes demonstrated a significantly higher-level of ALP activity compared with the control group. Moreover, it was demonstrated that cells treated with BMSCs-exosomes (40 μl) demonstrated significantly higher levels of cell death compared with the cells treated with the PBS (20 μl) and BMSCs-exosome (20 μl) mixture. These data further indicated an association between the amount of exosomes and ALP activity in BMSCs after osteogenic induction. Calcium nodule formation and high ALP activity in cells treated with high levels of exosomes further indicated their role in osteogenic differentiation.

To evaluate if BMSCs-exosomes had the potential to enhance BMSCs proliferation, the CCK-8 assay was used to evaluate the OD value for each cell culture sample after passage 4, which reflected indirectly, the extent of cell proliferation. A positive association between the proliferation of BMSCs and concentration of exosomes was demonstrated (Fig. 3F). Cell cultures containing exosomes promoted higher proliferation of BMSCs than controls containing no exosomes. Furthermore, the OD value for each cell culture increased as the number of exosomes added to the medium increased. The data presented were representative of triplicate experiments for all groups. These results indicated that exosome treatment not only promoted BMSCs proliferation, but also had the potential to accelerate this process at higher doses.

Characteristics of pTa. The pTa module used in the present study was flat and cylinder-shaped, approximately 3 mm in diameter (Fig. 4A) and 2 mm in height (Fig. 4B). The surface was comprised of interlinked three-dimensional honeycomb pores. The surface structures of pTa were imaged using SEM (Fig. 4C). SEM results showed that the internal micropores of pTa were cross-linked with each other, with pore gaps of ~500 μm and a pore size of ~80%.

Bone cavity repair assessment. Micro-CT scans were used to observe the osteogenic effect associated with the scaffold at 4, 8 and 12 weeks post-surgery (Fig. 5A). At 4 weeks, no marked increase in osteogenic activity was demonstrated in the NC group, with a small amount of bone callus formed; however, the bone cavity was still clearly visible. It should be noted that markedly more regenerative growth was demonstrated in the PE group compared with NC, Exo groups.

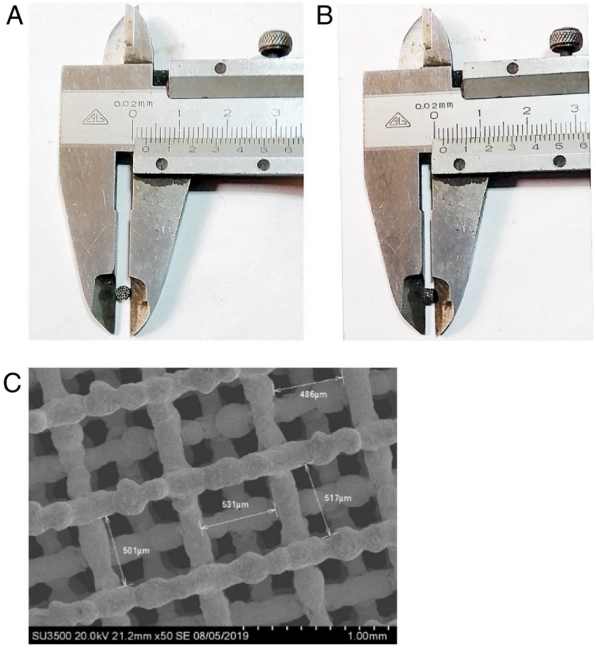

Figure 4. Characterization of the pTa module. Morphological measurement of the (A) diameter and (B) height of the porous tantalum modules. (C) Internal microstructure of porous tantalum module was assessed using.

At 8 weeks, new bone was beginning to form in all samples compared with week 4. Only minimal cell growth was observed in the NC and Exo groups, whereas markedly more growth was observed in the PT group containing scaffolds; however, this growth was markedly less than that of the PE treated group. At 12 weeks, the bone cavity in the NC group was filled; however, the micro-CT demonstrated low bone density compared with the control group, as well as a lack of contact with the scaffold. There was no marked difference demonstrated between the NC and Exo groups. The bone density of new bone around the implant material in the PT group was close to the control group; however, there was still as small gap between the new bone and the implant. In the PE treated group, the newly formed bone around the implant was similar to natural bone, which suggested that bone growth was stimulated with the pTa scaffold and exosomes compared with the other groups. Based on the micro-CT scans, a column diagram of the volume fraction of new bone at different time points was constructed (Fig. 5B). The PE group had a better osteogenic value at 4, 8 and 12 weeks compared with the other groups during the same period, which indicated better bone repair due to the combined pTa scaffold and exosome treatment.

Histological images of Gieson staining of each bone cavity at 12 weeks post-surgery presented bones from the NC group which contained few and scattered new bone trabeculae surrounding blue-stained fibrous tissues at the edge of each cavity (Fig. 6A and B). In contrast, the amount of newly formed bone was evident in bone treated with exosomes (Fig. 6C and D). These bones contained a more compact fiber structure than the other groups. However, it should be noted that in both the NC and Exo groups, there were large areas containing fibrous connective tissue. Implants in the PT and PE groups were observed to be

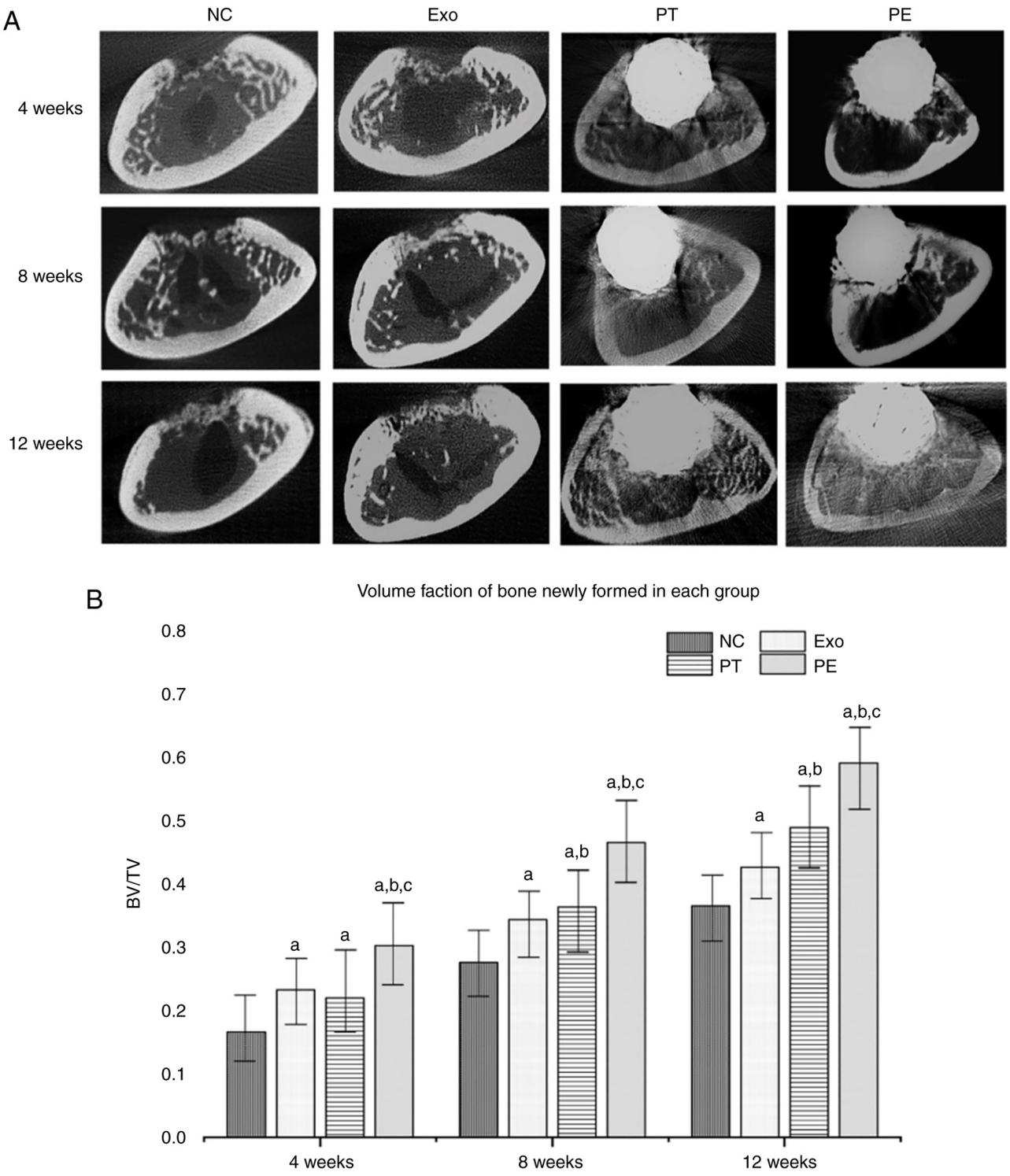

Figure 5. Imaging assessment of bone regeneration in defect sites. (A) Micro-CT images of the supracondylar femur of rats at 4, 8 and 12 weeks after surgery. (B) New bone volume fraction in each group at 4, 8 and 12 weeks postoperatively. [a]P<0.05 vs. NC; [b]P<0.05 vs. Exo; [c]P<0.05 vs. PT. pTa, tantalum metal; NC, no treatment control group; Exo, treated with exosomes; PT, treated with pTa; PE, treated with combined pTa and exosomes; BV/TV, bone volume/tissue volume.

compatible with bone tissue and remained in appropriate positions (Fig. 6E and G). Most importantly, the PT and PE groups contained a higher amount of calcium salt deposition, high levels of cartilage formation and high levels of osteoblasts (Fig. 6F and H). New bone mass and maturity gradually increased at the interface and inside the inner pores of the scaffold in the PT and PE groups, which indicated the biocompatibility and osteogenic ability of pTa. Notably, there was a visible seam between the scaffold and adjacent bone in PT group while the interface between the bone tissue and pTa was more uniform and smooth in the PE group, which indicated that the bone integration of pTa was further enhanced after being combined with exosomes (Fig. 6E-H). These results demonstrated that pTa combined with exosomes had the potential to accelerate the formation of new bone at 12 weeks post-implantation.

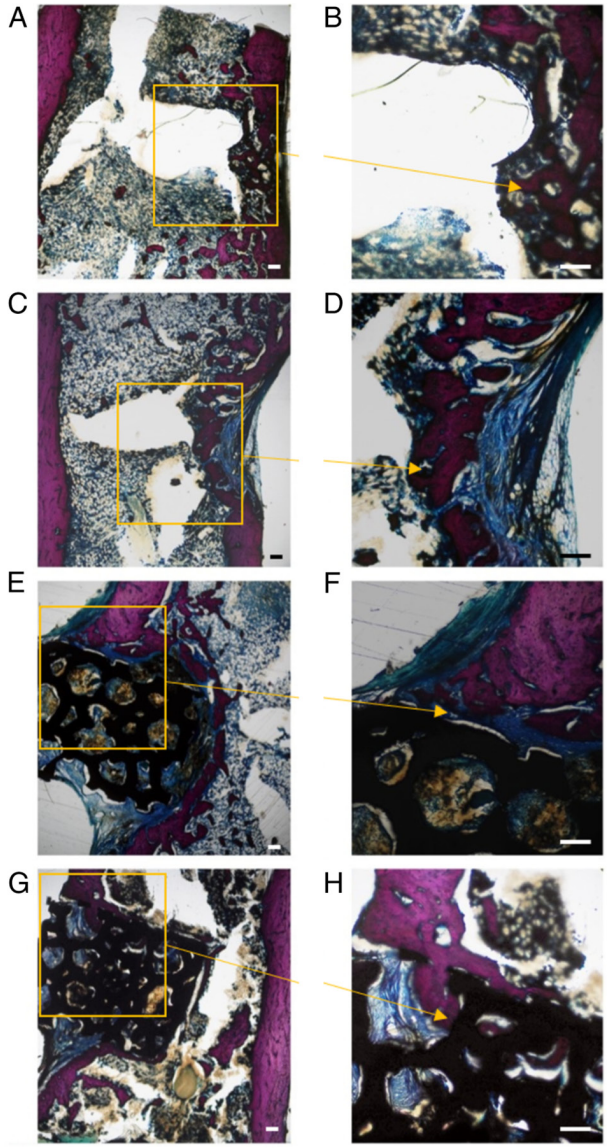

Figure 6. Histological assessment of bone regeneration in defect sites. Representative histological sections in each group at 12 weeks after surgery. (A and B) NC group: The defect area is empty with few bone trabeculae at the edges. (C and D) Exo Group: The defect area is filled with newly formed bone trabeculae and a large amount of fibrous tissue. (E and F) PT Group: The pTa is well integrated with the defect area. (G and H) PE Group: The pTa is excellently integrated with the defect area, and the surrounding new bone tissue has grown into the hole. Scale bar=200 μm. pTa, tantalum metal; NC, no treatment control group; Exo, treated with exosomes; PT, treated with pTa; PE, treated with combined pTa and exosomes; BV/TV, bone volume/tissue volume.

Discussion

Challenges to large bone defect repair include high incidence rate, requirement for a long course of treatment and difficulties, such as physical disability, promoted by deep lesions (29). Exosomes have great potential in the field of bone defect repair due to properties, such as promotion of tissue repair and angiogenesis, improvement of the local cell microenvironment and low immunogenicity (3,25,30). Wang *et al* (31) recently reported that BMSCs-exosomes immobilized on a titanium (Ti) surface had the potential to enhance BMSCs adhesion and proliferation, and upregulate stromal cell-derived factor gene expression. Exosomes have the potential to be designed for drug delivery based to their properties in order to increase efficacy. Liu *et al* (32) recently reported that exosomes derived from bacteria have the potential to be bioactive nanocarriers for drug delivery to damaged bones. BMSCs-exosomes have been reported to serve a role in BMSCs paracrine signaling, specifically in the bone tissue repair process, which indicated a protective effect (25). However, the mechanism of how exosomes influence BMSCs is still unclear. A recent study reported that exosomes secreted by BMSCs contain miRNAs related to osteogenesis, which may be partly responsible for inducing osteogenic differentiation of receptor BMSCs (33). Zhang *et al* (28) reported that BMSCs-exosomes have the potential to promote osteogenic differentiation through the activation of the BMP-2/Smad1/RUNX2 signaling pathway, which may be one of the underlying mechanisms in bone fracture healing. The present study demonstrated that as the concentration of the BMSCs-exosomes increased, so did calcium nodule deposition as shown through Alizarin red and ALP staining (Fig. 3E). Furthermore, alkaline phosphatase activity was demonstrated to be increased and cell proliferation to be accelerated. Thus, it could be hypothesized that BMSCs-exosomes serve an important role in improving the proliferation and differentiation of BMSCs. Researchers have previously generated certain engineered exosomes through modification, to obtain more efficient and accurate therapeutic effects (34). Hu *et al* (35) constructed engineered exosomes from NIH-3T3 cells that highly expressed a C-X-C motif chemokine receptor 4 and combined them with liposomes carrying antiagmir-188, which would allow for targeted drug released and promotion of the osteogenesis of bone marrow stromal cells, as well as inhibition of fat production. Lin *et al* (36) constructed a specific gene-activated exosome that could effectively modulate the gene release of vascular endothelial growth factor 165, as well as serve a role in enhancing therapy for vascular bone regeneration.

Bone tissue engineering typically requires bioactive materials for mechanical support and loading of bioactive factors. Swanson *et al* recently reported the loading of exosomes on poly(lactic-co-glycolic acid) and poly(ethylene glycol) triblock copolymer microspheres and incorporated them into a nanofiber poly(l-lactic acid) scaffold, which allowed for the local and controlled release of exosomes into the tissue, which protected their bioactivity (37). Furthermore, Ma *et al* (38) reported that bioactive factors loaded on pTa had slow-release properties that promote osteogenesis. In the present study, exosomes were loaded on pTa scaffolds and implanted into the bone defect to evaluate if they served a synergistic role in the promotion of bone regeneration. The data indicated that from 4 to 8 weeks post-surgery the rate of new bone growth was much lower in the EXO group compared with PT and PE groups, this could be because the BMSCs-exosomes were rendered inoperable once applied to bone defects, which lead to ineffective drug delivery to the area. Furthermore, the volume fraction of new bone in the PE group was significantly higher than in the other groups, with bone growth higher than that of the PT group 4-8 weeks post-surgery. This suggested that pTa was able to effectively prevent degradation or inactivation of exosomes resulting in more efficient bone regeneration. Nevertheless, the

release curve of the exosomes was not assessed in the present study and remains to be elucidated.

Many materials have been reported to show promise in the promotion of bone regeneration in animal models (39,40). For example, titanium (Ti) is a common metal implant material, which was has been reported to promote cell adhesion, proliferation and bone tissue regeneration, and is widely used in clinic practice (41). However, the intrinsic properties of Ta affords greater biocompatibility for BMSCs and improves overall osteogenesis compared with Ti (42-44). Thus, the present study used Ti as the carrier of choice to repair bone defects in the models used. Previous studies have reported excellent biocompatibility, bone growth and sufficient mechanical strength using pTa (45,46). Zhao *et al* (14,47) used pTa manufactured via 3-dimensional printing and chemical deposition technology to treat femoral head necrosis in the clinic. This indicated that pTa not only had the ability to act as an excellent scaffold, but also to act as a major mediator of osteoblast proliferation and growth for bone defects. The results of the CT scans in the present study (Fig. 5A) demonstrated mature osteocytes around the pTa material resembling normal bone tissue 12 weeks post-operation in the pTa-exosome treated group. Notably, a large amount of the new bone adhered tightly to the scaffold without obvious gaps. The results of previous reports and the present study both suggest superior biocompatibility can be achieved with pTa.

pTa has previously been reported to be beneficial for bone growth and bone-implant fixation in *in vivo* models (43). Images of Gieson staining of bone tissue samples at 12 weeks post-surgery were captured for evaluation and analysis (Fig. 6). These data demonstrated sparse and scattered nascent trabeculae formation in the NC group, while the exosome and PT groups expressed tightly integrated trabeculae, further illustrating the osteoinductive properties of BMSCs-exosomes and pTa. Interestingly, the thickness and regularity of nascent bone trabeculae was significantly better in the PE group compared with the others, which suggested a trend of bone tissue regeneration. In the PE group the new bone tissue not only tightly wrapped around the surface of the scaffold but also grew into the internal pores, while the rest of the pores were occupied by fibrous connective tissue, which further improved the stability of the implant. The microscopy results were consistent with the micro-CT scans. Based on the above histological and imaging results, it is possible to attribute the excellent bone integration and regeneration of the PE group to the synergistic effects of exosome therapy and pTa.

In summary, all of our studies have demonstrated that exosomal therapy combined with pTa can improve bone regeneration of femur defects in rats by promoting osteogenesis. However, the relationship between the quantity and concentration of exosomes and the amount of newly formed bone needs to be investigated more thoroughly in future studies.

In conclusion it is known that long-term preclinical testing for decades is required to create engineering scaffolds for use in clinical practice. One of the most important factors in implantation and cellular therapy is patient safety. Using the approach reported in the present study, pTa combined with BMSCs-exosomes had no inhibitory effect on the proliferation of BMSCs *in vitro* and also promoted the adhesion and differentiation of autologous cells. Furthermore, the *in vivo* studies demonstrated that exosomes and pTa could be leveraged for bone regeneration with a high degree of safety, effectiveness and simplicity. This work demonstrated the potential for significant clinical advancement for the repair of large bone defects in the future.

Acknowledgements

Not applicable.

Funding

This work was supported by The China Postdoctoral Science Foundation (grant no. 285395), The Dalian Medical Science Research Project (grant no. 2111038), Dalian Key Medical Specialties 'Peak Climbing' Program 2021 (grant no. 243) and The National Natural Science Foundation of China (grant no. 82172398).

Availability of data and materials

The datasets used and/or analyzed during the current study are available from the corresponding author on reasonable request.

Authors' contributions

BL and DZ conceived and designed the experiments. HC, SM, JL, YL, CL and JY performed the experiments. FY and MW analyzed the data. FY and BL confirm the authenticity of all the raw data. FY and MW were major contributors in writing the manuscript. All authors read and approved the final manuscript.

Ethics approval and consent to participate

The animal experiments (approval no. 201612009) were all performed according to the standards of The Animal Ethics Committee of The Affiliated Zhongshan Hospital of Dalian University.

Patient consent for publication

Not applicable.

Competing interests

The authors declare that they have no competing interests.

References

1. Jeon YS, Jeong HY, Lee DK, Rhee YG: Borderline glenoid bone defect in anterior shoulder instability: Latarjet procedure versus bankart repair. Am J Sports Med 46: 2170-2176, 2018.
2. Inglis S, Schneider KH, Kanczler JM, Redl H and Oreffo ROC: Harnessing human decellularized blood vessel matrices and cellular construct implants to promote bone healing in an ex vivo organotypic bone defect model. Adv Healthc Mater 8: e1800088, 2019.
3. Iordachescu A, Hulley P and Grover LM: A novel method for the collection of nanoscopic vesicles from an organotypic culture model. RSC Adv 8: 7622-7632, 2018.

4. Gleeson JP, Plunkett NA and O'Brien FJ: Addition of Hydroxyapatite Improves Stiffness, Interconnectivity And Osteogenic Potential Of A Highly Porous Collagen-Based Scaffold For Bone Tissue Regeneration. Eur Cell Mater 20: 218-230, 2010.
5. Ghanaati S, Barbeck M, Booms P, Lorenz J, Kirkpatrick CJ and Sader RA: Potential lack of 'standardized' processing techniques for production of allogeneic and xenogeneic bone blocks for application in humans. Acta Biomater 10: 3557-3562, 2014.
6. Andrzejowski P, Masquelet A and Giannoudis PV: Induced Membrane Technique (Masquelet) for bone defects in the distal tibia, foot, and ankle: systematic review, case presentations, tips, and techniques. Foot Ankle Clin 25: 537-586, 2020.
7. Bouguennec N and Colombet P: Iterative rupture of the patellar tendon: A case report of an original technique for revision reconstruction using an adjustable loop and an artificial ligament. Case Rep Orthop 2018: 6107287, 2018.
8. Henkel J, Woodruff MA, Epari DR, Steck R, Glatt V, Dickinson IC, Choong PF, Schuetz MA and Hutmacher DW: Bone regeneration based on tissue engineering conceptions-A 21st century perspective. Bone Res 1: 216-248, 2013.
9. Langer R and Vacanti JP: Tissue engineering. Science 260: 920-926, 1993.
10. Wu S, Liu X, Yeung KWK, Liu C and Yang X: Biomimetic porous scaffolds for bone tissue engineering. Mater Sci Eng R-Rep 80: 1-36, 2014.
11. Stiehler M, Lind M, Mygind T, Baatrup A, Dolatshahi-Pirouz A, Li H, Foss M, Besenbacher F, Kassem M and Bünger C: Morphology, proliferation, and osteogenic differentiation of mesenchymal stem cells cultured on titanium, tantalum, and chromium surfaces. J Biomed Mater Res A 86: 448-458, 2008.
12. Levine BR, Sporer S, Poggie RA, Della Valle CJ and Jacobs JJ: Experimental and clinical performance of porous tantalum in orthopedic surgery. Biomaterials 27: 4671-4681, 2006.
13. Findlay DM, Welldon K, Atkins GJ, Howie DW, Zannettino AC and Bobyn D: The proliferation and phenotypic expression of human osteoblasts on tantalum metal. Biomaterials 25: 2215-2227, 2004.
14. Zhao D, Zhang Y, Wang W, Liu Y, Li Z, Wang B and Yu X: Tantalum rod implantation and vascularized iliac grafting for osteonecrosis of the femoral head. Orthopedics 36: 789-795, 2013.
15. Zhao D, Cui D, Wang B, Tian F, Guo L, Yang L, Liu B and Yu X: Treatment of early stage osteonecrosis of the femoral head with autologous implantation of bone marrow-derived and cultured mesenchymal stem cells. Bone 50: 325-330, 2012.
16. Herberts CA, Kwa MS and Hermsen HP: Risk factors in the development of stem cell therapy. J Transl Med 9: 29, 2011.
17. Amariglio N, Hirshberg A, Scheithauer BW, Cohen Y, Loewenthal R, Trakhtenbrot L, Paz N, Koren-Michowitz M, Waldman D, Leider-Trejo L, *et al*: Donor-derived brain tumor following neural stem cell transplantation in an ataxia telangiectasia patient. PLoS Med 6: e1000029, 2009.
18. Kansu E: Thrombosis in stem cell transplantation. Hematology 17 (Suppl 1): S159-S162. 2012.
19. Valadi H, Ekstrom K, Bossios A, Sjostrand M, Lee JJ and Lotvall JO: Exosome-mediated transfer of mRNAs and microRNAs is a novel mechanism of genetic exchange between cells. Nat Cell Biol 9: 654-659, 2007.
20. Braicu C, Tomuleasa C, Monroig P, Cucuianu A, Berindan-Neagoe I and Calin GA: Exosomes as divine messengers: Are they the Hermes of modern molecular oncology? Cell Death Differ 22: 34-45, 2015.
21. Li J, Liu K, Liu Y, Xu Y, Zhang F, Yang H, Liu J, Pan T, Chen J, Wu M, *et al*: Exosomes mediate the cell-to-cell transmission of IFN-α-induced antiviral activity. Nat Immunol 14: 793-803, 2013.
22. Qi X, Zhang J, Yuan H, Xu Z, Li Q, Niu X, Hu B, Wang Y and Li X: Exosomes secreted by human-induced pluripotent stem cell-derived mesenchymal stem cells repair critical-sized bone defects through enhanced angiogenesis and osteogenesis in osteoporotic rats. Int J Biol Sci 12: 836-849, 2016.
23. Zhang J, Liu X, Li H, Chen C, Hu B, Niu X, Li Q, Zhao B, Xie Z and Wang Y: Exosomes/tricalcium phosphate combination scaffolds can enhance bone regeneration by activating the PI3K/Akt signaling pathway. Stem Cell Res Ther 7: 136, 2016.
24. Zhang S, Chu WC, Lai RC, Lim SK, Hui JH and Toh WS: Exosomes derived from human embryonic mesenchymal stem cells promote osteochondral regeneration. Osteoarthritis Cartilage 24: 2135-2140, 2016.
25. Furuta T, Miyaki S, Ishitobi H, Ogura T, Kato Y, Kamei N, Miyado K, Higashi Y and Ochi M: Mesenchymal stem cell-derived exosomes promote fracture healing in a mouse model. Stem Cells Transl Med 5: 1620-1630, 2016.
26. Guan S, Yu H, Yan G, Gao M, Sun W and Zhang X: Characterization of urinary exosomes purified with size exclusion chromatography and ultracentrifugation. J Proteome Res 19: 2217-2225, 2020.
27. Gao J, Zhang G, Xu K, Ma D, Ren L, Fan J, Hou J, Han J and Zhang L: Bone marrow mesenchymal stem cells improve bone erosion in collagen-induced arthritis by inhibiting osteoclasia-related factors and differentiating into chondrocytes. Stem Cell Res Ther 11: 171, 2020.
28. Zhang L, Jiao G, Ren S, Zhang X, Li C, Wu W, Wang H, Liu H, Zhou H and Chen Y: Exosomes from bone marrow mesenchymal stem cells enhance fracture healing through the promotion of osteogenesis and angiogenesis in a rat model of nonunion. Stem Cell Res Ther 11: 38, 2020.
29. Faldini C, Traina F, Perna F, Borghi R, Nanni M and Chehrassan M: Surgical treatment of aseptic forearm nonunion with plate and opposite bone graft strut. Autograft or allograft? Int Orthop 39: 1343-1349, 2015.
30. Qin Y, Sun R, Wu C, Wang L and Zhang C: Exosome: A novel approach to stimulate bone regeneration through regulation of osteogenesis and angiogenesis. Int J Mol Sci 17: 712, 2016.
31. Wang X, Shah FA, Vazirisani F, Johansson A, Palmquist A, Omar O, Ekström K and Thomsen P: Exosomes influence the behavior of human mesenchymal stem cells on titanium surfaces. Biomaterials 230: 119571, 2020.
32. Liu H, Zhang Q, Wang S, Weng W, Jing Y and Su J: Bacterial extracellular vesicles as bioactive nanocarriers for drug delivery: Advances and perspectives. Bioact Mater 14: 169-181, 2021.
33. Wang XQ, Omar O, Vazirisani F, Thomsen P and Ekstrom K: Mesenchymal stem cell-derived exosomes have altered microRNA profiles and induce osteogenic differentiation depending on the stage of differentiation. PLoS One 13: e0193059, 2018.
34. Ma S, Zhang Y, Li S, Li A, Li Y and Pei D: Engineering exosomes for bone defect repair. Front Bioeng Biotechnol 10: 1091360, 2022.
35. Hu Y, Li X, Zhang Q, Gu Z, Luo Y, Guo J, Wang X, Jing Y, Chen X and Su J: Exosome-guided bone targeted delivery of Antagomir-188 as an anabolic therapy for bone loss. Bioact Mater 6: 2905-2913, 2021.
36. Lin T, Zha Y, Zhang X, Chen J, Li Y, Wang Z, Zhang S, Wang J and Li Z: Gene-activated engineered exosome directs osteoblastic differentiation of progenitor cells and induces vascularized osteogenesis in situ. Chem Eng J 400: 125939, 2020.
37. Swanson WB, Zhang Z, Xiu K, Gong T, Eberle M, Wang Z and Ma PX: Scaffolds with controlled release of pro-mineralization exosomes to promote craniofacial bone healing without cell transplantation. Acta Biomater 118: 215-232, 2020.
38. Ma L, Cheng S, Ji X, Zhou Y, Zhang Y, Li Q, Tan C, Peng F, Zhang Y and Huang W: Immobilizing magnesium ions on 3D printed porous tantalum scaffolds with polydopamine for improved vascularization and osteogenesis. Mater Sci Eng C Mater Biol Appl 117: 111303, 2020.
39. Shi Y, He R, Deng X, Shao Z, Deganello D, Yan C, and Xia Z: Three-dimensional biofabrication of an aragonite-enriched self-hardening bone graft substitute and assessment of its osteogenicity in vitro and in vivo. Biomater Transl 1: 69-81, 2020.
40. Jing X, Ding Q, Wu Q, Su W, Yu K, Su Y, Ye B, Gao Q, Sun T and Guo X: Magnesium-based materials in orthopaedics: Material properties and animal models. Biomater Transl 2: 197-213, 2021.
41. Liu B, Ma Z, Li J, Xie H, Wei X, Wang B, Tian S, Yang J, Yang L, Cheng L, *et al*: Experimental study of a 3D printed permanent implantable porous Ta-coated bone plate for fracture fixation. Bioact Mater 10: 269-280, 2021.
42. Lu MM, Wu PS, Guo XJ, Yin LL, Cao HL and Zou D: Osteoinductive effects of tantalum and titanium on bone mesenchymal stromal cells and bone formation in ovariectomized rats. Eur Rev Med Pharmacol Sci 22: 7087-7104, 2018.
43. Wang H, Su K, Su L, Liang P, Ji P and Wang C: Comparison of 3D-printed porous tantalum and titanium scaffolds on osteointegration and osteogenesis. Mater Sci Eng C Mater Biol Appl 104: 109908, 2019.

44. Lu M, Zhuang X, Tang K, Wu P, Guo X, Yin L, Cao H and Zou D: Intrinsic surface effects of tantalum and titanium on integrin α5β1/ERK1/2 pathway-mediated osteogenic differentiation in rat bone mesenchymal stromal cells. Cell Physiol Biochem 51: 589-609, 2018.
45. Dou X, Wei X, Liu G, Wang S, Lv Y, Li J, Ma Z, Zheng G, Wang Y, Hu M, *et al*: Effect of porous tantalum on promoting the osteogenic differentiation of bone marrow mesenchymal stem cells in vitro through the MAPK/ERK signal pathway. J Orthop Transl 19: 81-93, 2019.
46. Wei X, Liu B, Liu G, Yang F, Cao F, Dou X, Yu W, Wang B, Zheng G, Cheng L, *et al*: Mesenchymal stem cell-loaded porous tantalum integrated with biomimetic 3D collagen-based scaffold to repair large osteochondral defects in goats. Stem Cell Res Ther 10: 72, 2019.
47. Zhao D, Liu B, Wang B, Yang L, Xie H, Huang S, Zhang Y and Wei X: Autologous bone marrow mesenchymal stem cells associated with tantalum rod implantation and vascularized iliac grafting for the treatment of end-stage osteonecrosis of the femoral head. Biomed Res Int 2015: 240506, 2015.